Multi-omics analysis reveals dermokine as a regulator of keratinocyte differentiation and adhesion

Vahap Canbay[1], Till Wüstemann[2], Weihua Tian[1], Tobias A. Beyer[3], Camilla Reiter Elbæk[1], Michael Stumpe[6], Gaetana Restivo[5], Chatpakorn Christiansen[1], Anabel Migenda Herranz[3], Susanne Mailand[3], Jürg Hafner[5], Rune Busk Damgaard[1], Steffen Goletz[1], Jörn Dengjel[4], Ulrich auf dem Keller[1, †] and Chiara Francavilla[1, 6, *]

[1]Department for Bioengineering and Biomedicine, Technical University of Denmark, 2800, Copenhagen, Denmark.

[2]Department of Biology, Swiss Federal Institute of Technology Zurich, 8152, Zurich, Switzerland.

[3]Cytosurge AG, Glattbrugg, 8152, Zurich, Switzerland.

[4]Department of Biology, University of Fribourg, 1700, Fribourg, Switzerland.

[5]Department of Dermatology, University Hospital Zurich, 8091, Zurich, Switzerland

[6]Division of Cellular and Molecular Function, FBMH, The University of Manchester, M139PT, United Kingdom

[†]Deceased

*Corresponding author: Chiara Francavilla. Department for Bioengineering and Biomedicine, Technical University of Denmark, Søitofts Plads, 2800, Kongens Lyngby, Denmark. Phone: 004593511641 E-mail: chiafra@dtu.dk

Keywords: dermokine, epithelial differentiation, p120, catenin, cadherin binding, cell-cell adhesion, functional phosphoproteomics, multi-omics, three-dimensional organotypic skin cultures, non-healing wounds

Abstract

Impaired adhesion and differentiation of keratinocytes is a hallmark of several skin diseases, but only some of the factors that regulate these processes have been identified. Here, we studied the role of isoform-rich dermokine – a wound- and tumor-regulated protein – in keratinocytes using a combination of multi-omics and functional approaches. CRISPR/Cas9-induced knockout of dermokine isoforms in human keratinocytes inhibited differentiation of these cells in three-dimensional organotypic skin cultures, which was confirmed by quantitative proteomics. In two-dimensional monocultures, dermokine deficiency affected the proteome and phosphoproteome as revealed by mass spectrometry. We found reduced abundance of differentiation-specific proteins and increased phosphorylation of cell adhesion protein p120 (cateninδ1). The adhesive strength of dermokine knockout keratinocytes was impaired, which was rescued by p120 knock-down or ROCK inhibition. Finally, we verified the correlation between decreased dermokine expression and increased p120 phosphorylation in human non-healing wounds. These results identify dermokine as regulator of keratinocyte adhesion and differentiation, involving at least in part its effect on p120 phosphorylation and ROCK. Our data point to a function of dermokine in the pathogenesis of chronic wounds.

Introduction

The skin is the largest organ of the human body and is composed of epidermis, dermis and subcutis(1). Keratinocytes, the most prominent cell type of the epidermis, form a stratified epithelium through their gradual differentiation (2). The epidermis serves as a protective barrier against external threats, water loss, and mechanical strain (1). Therefore, impaired keratinocyte differentiation and epidermal stratification have severe consequences and are a hallmark of a plethora of skin diseases, such as psoriasis, epithelial skin cancers and non-healing wounds (3). In squamous cell carcinomas (SCCs), keratinocytes lose the ability to differentiate into a stratified epithelium and undergo epithelial to mesenchymal transition (EMT) mediated by the loss of cell-cell adhesion proteins (4). In psoriatic tissue, keratinocytes are exposed to high levels of inflammatory cytokines, causing excessive proliferation and aberrant differentiation (5). Further, in the context of non-healing wounds, keratinocytes at the wound edge remain in a vicious cycle of chronic inflammation, which also affects the wound bed. This prevents keratinocytes to migrate and to re-epithelialize the wound (6–8). In summary, keratinocyte function must be tightly regulated to prevent such devastating diseases, and a deeper understanding of the molecular determinants underlying keratinocyte function, including their differentiation process, will open new avenues for the treatment of skin diseases.

Several molecules have been described as regulators of keratinocyte differentiation, including growth factors, calcium, and proteases (9, 10). Specifically, changes in the abundance, activity, substrate availability, as well as inhibition of protease activities have been associated with keratinocyte differentiation. Among the relevant players are kallikrein-related peptides (KLK), the desquamation cascade, and the cathepsin-induced activation of transglutaminases (TGM) (9). Studying the protease substrate repertoire is important for the understanding of keratinocyte differentiation (9). Among proteases with a function in keratinocytes, the wound and cancer-associated matrix metalloproteinase 10 (MMP10), which is expressed in wound-edge keratinocytes of skin lesions, plays a crucial role in the cleavage of proteins regulating keratinocyte migration and adhesion (11, 12). We have previously identified dermokine, a member of the stratified epithelium-secreted peptide complex, as a substrate of MMP10 in basal keratinocytes (12). Dermokine is expressed by differentiating keratinocytes, absent in the basal layer, minimally present in the spinous layer, and most abundant in the granular layer (13). Even though a role of dermokine in modulating keratinocyte differentiation in mice has been suggested (14), the functions and mechanisms of action of dermokine in human keratinocytes remain unknown. This is relevant because of the multiple differences between murine and human epidermis (15, 16).

Dermokine is encoded by the *DMKN* gene, which encodes three major protein isoforms: dermokine-α, -β, and -γ (17). Alternatively spliced dermokine-β and -γ, which are generated from the same hnRNA, are secreted into the extracellular space and found in the granular layer of the epidermis, whereas the dermokine-α RNA transcription is initiated 11739 nucleotides further downstream and expressed. This isoform is expressed at similar levels throughout all epidermal layers (13, 18). In mice, knockout of dermokine-β and γ caused neonatal skin hyperkeratosis, resembling psoriasis-like skin disorders (14). As mice deficient in all dermokine isoforms show a more severe phenotype, dermokine-α is likely to compensate for the loss of the other isoforms during keratinocyte differentiation (14). Here, to reveal the role of dermokine in keratinocyte differentiation in the human context, we generated human keratinocytes with CRISPR/Cas9-mediated knockout of different dermokine isoforms and characterized their behaviour in three-dimensional (3D) organotypic skin cultures (19, 20). These 3D cultures form epidermis-like structures, including the presence of differentiating keratinocytes, and have been widely used as an experimental model to study the mechanisms underlying skin diseases, including SCC (21, 22). To characterize the functions of DMKN in keratinocyte differentiation, these genetically engineered 3D cultures were analyzed by quantitative multi-omics approaches, and the results were validated by functional assays in vitro and in vivo. We show that dermokine knockout affects the expression of epidermal proteins in 3D cultures, including p120, a known regulator of cell-cell adhesion (23). In summary, multi-omics, functional analyses of keratinocyte models and skin tissue staining revealed that dermokine regulates differentiation and cell-cell adhesion of keratinocytes.

Results

Dermokine is important for early keratinocyte differentiation in 3D skin equivalents

To study a possible role of dermokine in keratinocyte differentiation (12), we edited the genomic sites coding for either dermokine-β/γ or -α/β (*DMKN* βγ or αβ) in human keratinocytes by two different CRISPR/Cas9 methods (19, 24) (Figure 1A). The immortalized, but non-tumorigenic N/TERT keratinocyte cell line was used for this purpose, because it undergoes normal differentiation and stratification in 3D skin equivalents and allows the generation of clonally-expanded lines (25).The first method, “chemical transfection”, which is based on fluorescence-activated cell sorting (FACS) of single-cell clones and clonal expansion, generated the *DMKN* βγ-/- cell line (26) (Figure 1B). The second method, “FluidFM™ CRISPR approach”, which was based on co-injecting CRISPR ribonucleoprotein (RNP) and green fluorescent protein (GFP) mRNA into keratinocytes, generated the *DMKN* αβ-/- cell line (27) (Figure 1C). We confirmed the lack of expression of *DMKN* generated with either method by Sanger sequencing (28) (Supplemental Figure 1A-D). We then established 3D organotypic skin cultures by plating either WT or *DMKN* βγ-/- or *DMKN* αβ-/- keratinocytes on top of primary human fibroblasts incorporated in matrigel, as previously described(19) (Figure 1B-C). Under these conditions, keratinocytes form a multilayered, stratified epidermis, resembling human skin(19). We evaluated whether changing the calcium concentration in our experimental conditions from 1 mM to 5 mM affects cell proliferation and differentiation by staining for the keratin 14 (KRT14), a marker for non-differentiated keratinocytes, and for the early differentiation marker KRT10 (Supplemental Figure 1E). Quantification of immunofluorescence stainings for KRT10 and KRT14 in varying calcium concentrations showed that the differentiation marker KRT10 did not change, while KRT14 levels decreased in response to elevated calcium (Supplemental Figure 1E). These results suggest that cells undergo the differentiation program in 3D organotypic skin culture, giving rise to a stratified, epidermis-like structure. To confirm changes in the expression of dermokine isoforms in this model system at the protein level, we could not use immunoblotting due to the lack of antibodies recognizing the specific isoforms. Instead, we used targeted proteomics and synthetic reference peptides (29, 30). We selected five proteotypic peptides spread across the entire dermokine sequence, including two near the N-terminus, two after the keratin-like domain, and one at the C-terminus (Figure 1D, Supplemental Table 1). As the C-terminal peptide GGVSPSSSASR is shared by both dermokine-β and -α (Figure 1D), deletion of the sole dermokine-β/γ isoform would still give a signal in the mass spectrometer (MS) because of the expression of the α isoform. Indeed, only a slight reduction in the peptide peak area was observed when only isoforms -β

and -γ were genetically deleted (Figure 1E, Supplemental Figure 1F and Supplemental Table 1). However, removing the dermokine-α and -β isoforms simultaneously resulted in a substantial decrease in the abundance of such a shared C-terminal peptide (Figure 1F, Supplemental Figure 1F and Supplemental Table 1). Among the remaining four peptides, the N-terminal peptide VGEAAHALGNTGHEIGR showed the highest decrease in abundance upon depletion of both *DMKN* βγ and *DMKN* αβ in 3D organotypic skin cultures (Supplemental Figure 1F-J and Supplemental Table 1). Then, we analyzed WT and *DMKN* KO 3D cultures by immunohistochemical (IHC) staining and showed the strong reduction of dermokine expression in both *DMKN* βγ-/- and *DMKN* αβ-/- compared to WT cultures (Figure 2). Hematoxylin and eosin (H/E) as well as IHC staining revealed the lack of suprabasal layers beyond the spinous layer in the *DMKN* KO compared to the WT samples (Figure 2). This observation was consistent with the known dermokine expression pattern in keratinocytes (13). Together, these data suggest that the expression of *DMKN* isoforms is indeed reduced at the protein level in our model system, which seems to affect keratinocyte differentiation.

Next, we evaluated whether the lack of dermokine affected the early-stage differentiation of keratinocytes by staining for KRT14 and KRT10(1). The expression of KRT14 was comparable in WT and in both *DMKN* KOs cultures, whereas the expression of KRT10 decreased in the KOs compared to the WT samples (1) (Figure 2). These data suggest that dermokine is important for early keratinocyte differentiation. The expression of integrin α 6 (ITGα6), a marker of basal keratinocytes(31), and of the proliferation marker Ki-67 were similar in WT and *DMKN* KO keratinocytes, suggesting that hemidesmosome formation and proliferation do not change upon dermokine depletion (1) (Figure 2). Altogether, the IHC analysis suggests that the *DMKN* KO reduces the amounts of differentiation-specific proteins.

Knockout of dermokine variants alters the keratinocyte proteome in organotypic skin cultures

To characterize the phenotype of *DMKN* KO samples in an unbiased manner, we analyzed changes in the proteome of the total 3D organotypic skin cultures grown from either WT or *DMKN* KO keratinocytes via quantitative liquid chromatography – mass spectrometry (LC-MS)-based proteomics. In total, we quantified 3753 proteins in WT, *DMKN* βγ-/- and *DMKN* αβ-/- 3D cultures with a coefficient of variation (CV) of less than 15 % between the replicates (Supplemental Figure 2A and Supplemental Table 2). The Pearson correlation analysis of WT, *DMKN* βγ-/- and *DMKN* αβ-/- 3D cultures revealed high correlation among replicates for each experimental condition (Supplemental Figure 2B), in line with previous publications (32, 33). Finally, principal

component analysis (PCA) demonstrated clear differences in the proteome of cultures with the three different genotypes (Supplemental Figure 3C). Hierarchical clustering identified clusters including proteins that are more abundant in the WT (Cluster 2), in both the KO (Cluster 4), or only in one of the two KO samples (Clusters 1 and 3) (Supplemental Figure 2D), suggesting individual, but also overlapping functions of the two dermokine isoforms in keratinocytes. Gene Ontology (GO) term enrichment analysis showed that proteins in Cluster 2 were enriched in terms like “formation of the cornified envelope” and proteins in Cluster 4 were associated with signaling pathways (Supplemental Figure 2E). The differential abundance analysis, visualized by Volcano plot, revealed 312 and 231 significantly more abundant proteins in the *DMKN* βγ-/- and *DMKN* αβ-/- 3D cultures, respectively, when compared to WT (Figure 3A and Supplemental Table 2). We also identified 217 and 230 significantly less abundant proteins in the respective *DMKN* βγ-/- and *DMKN* αβ-/- keratinocytes in comparison to the WT (Figure 3B and Supplemental Table 2). The protein abundance of dermokine and KRT10 was reduced in both *DMKN* KO 3D cultures, confirming the results of the IHC staining (Figures 2, 3A-B). KRT14, and ITGα6 showed no differential abundance in the *DMKN* βγ-/- clone, as seen in the IHC analysis, but were slightly increased in the *DMKN* αβ-/- clone (Figures 2 and 3A-B). Along with dermokine, the abundance of suprabasin (SBSN) and keratinocyte differentiation-associated protein (KRTDAP), which are all members of the stratified epithelium secreted peptides complex (SSC) expressed in the suprabasal layers of the stratified epithelium(34), was also reduced (Figure 3A-B). GO enrichment analysis of significantly less abundant proteins from both the *DMKN* KOs compared to WT clones showed the enrichment of pathways such as “keratinocyte differentiation” and “formation of the cornified envelope” (Figure 3C), whereas the GO enrichment analysis of significantly more abundant proteins showed the enrichment of “integrin binding, positive regulation of locomotion and growth factor binding pathways” (Figure 3D).

In conclusion, dermokine regulates the abundance of proteins of the suprabasal layers of the epidermis in human skin equivalents.

Phosphoproteomics analysis reveals that dermokine regulates cell-cell adhesion proteins

To uncover how loss of dermokine may affect keratinocyte differentiation, we studied changes in cellular signaling by deep quantitative proteomics and phosphoproteomics analyses of WT, *DMKN* αβ-/-, and *DMKN* βγ-/- keratinocytes in monocultures (referred to as *DMKN* αβ-/- and *DMKN* βγ-/, respectively). In addition, we tested if treatment of the KO samples with recombinant dermokine-β (35) rescues the alterations in the proteome and phosphoproteome.

We first focused on the proteome and found 5118 unique quantified proteins (Supplemental Table 3) with the median CV of the protein groups being below 20% for all samples and the correlation analysis showing high correlation between replicates, but clear differences between the different genotypes in the PCA analysis (Supplemental Figure 3B-D). The *DMKN* αβ-/- or *DMKN* βγ-/- proteomes differed from the WT proteome, as shown by hierarchical clustering (Supplemental Figure 4A), and this difference was not rescued by treatment with recombinant dermokine. When we subjected the significantly differentially abundant proteins in the different samples to GO enrichment analysis, we found several enriched GO terms, including the term "cadherin binding", reciprocally enriched in two conditions: when comparing the most abundant proteins from non-treated *DMKN* αβ-/- and *DMKN* βγ-/- cells to those from WT keratinocytes (Supplemental Figure 4B) and when comparing the significantly less abundant proteins from the dermokine-treated *DMKN* αβ-/- and *DMKN* βγ-/- cell lines to those from WT keratinocytes (Supplemental Figure 4C). These 2D results confirm that dermokine knockout changes the keratinocyte proteome (Figure 3).

Next, we analyzed changes in the phosphoproteome of non-treated and dermokine-treated *DMKN* βγ-/- and *DMKN* αβ-/- cell lines compared to WT keratinocytes (Supplemental Figure 3A and Supplemental Table 4). We enriched phosphorylated peptides using automated iron(III)-nitrilotriacetic acid (Fe(III)-NTA) and used a modified high-resolution MS-data independent acquisition (HRMS1)-DIA strategy covering a 400-1400 m/z mass range (36–38) (Supplemental Figure 5A). In total, we identified 11778 phosphorylation sites after filtering for localization site probability (≥ 0.75) and 4453 fully quantifiable phosphorylated sites across all conditions on 2695 proteins (Supplemental Figure 5B and Supplemental Table 4). All replicates showed high correlation scores (Supplemental Figure 5C), and we found 10027 single, 1367 double and 384 multiple phosphorylated sites (Supplemental Figure 5D) and 10315, 1164 and 299 phosphorylated serine, threonine and tyrosine amino acids, respectively (Supplemental Figure 5E). Overall, the quality of the phosphoproteomics datasets was consistent with previous publications(38). We observed significant differences between the phosphoproteome of *DMKN* βγ-/- and *DMKN* αβ-/- cell lines compared to the WT cell phosphoproteome (4453 phosphorylated sites) by hierarchical clustering (Supplemental Figure 5F). The phosphoproteome of dermokine-treated *DMKN* βγ-/- and *DMKN* αβ-/- keratinocytes was similar to the phosphoproteome of WT cells, suggesting a considerable reversal of the abnormal phosphorylation pattern of the KO keratinocytes upon treatment with recombinant dermokine (Supplemental Figure 5F). To study how dermokine affects cellular signaling, we applied a global Kinase-Substrate prediction approach(39), which reveals the likelihood of a kinase modifying

a phosphorylated site by linking kinase recognition sequence motifs and known in vivo and in vitro phosphorylation profiles(39) to the 4453 phosphorylated sites identified in the WT and the KO samples. This approach identified 94 putative kinases (Supplemental Table 5) whose known downstream phosphorylated sites were visualized in a heat map (Figure 4A). Among the 94 kinases and based on the kinase activity score, we identified 30 kinases with a high change and 15 kinases which showed significantly highest changes between the endogenous WT and all the *DMKN* βγ-/- and *DMKN* αβ-/- samples (Figure 4B and Supplemental Table 5). Four of the latter kinases were cytoplasmic tyrosine kinases (DYRK1A, PTK2B, SRC and SYK), of which both SRC and SYK showed decreased activity scores in the *DMKN* βγ-/- and *DMKN* αβ-/- keratinocytes compared to WT (Figure 4B). Similarly, our data showed a significantly higher activity scores of ROCK1, a key regulator of the cytoskeleton (40, 41) in KO keratinocytes relative to WT cells (Figure 4B). Next, we used the kinase-substrate annotations generated by the global kinase-substrate prediction approach to cluster substrates sharing similar kinase profiles and regulation(39) and we identified 8 clusters (Supplemental Figure 6 and Supplemental Table 5). Interestingly, each cluster had a different distribution of phosphorylated serine, threonine and tyrosine residues, ranging from cluster 2, 3, 4, and 6 not containing any phosphorylated tyrosines, to cluster 8 containing only phosphorylated serines, and clusters 5 and 7 mainly containing phosphorylated tyrosine and threonine sites, with cluster 7 being associated with PTK2B, ROCK1, SRC and SYK activity (Supplemental Figure 6). GO enrichment analysis of the 8 clusters revealed enrichment of terms related to “RNA regulation” in all clusters, specifically in cluster 7, which, together with cluster 2, also contained several proteins associated with “adherens junctions” and “cadherin binding” (Figure 4C). This finding is in line with SRC, a known player in cell-cell adhesion(42), being the most likely kinase regulating the proteins belonging to cluster 7 (Supplemental Figure 6) and with “cadherin binding” being the most strongly dysregulated pathway in the *DMKN* βγ-/- and *DMKN* αβ-/- keratinocytes compared to WT (Supplemental Figure 4). To identify potential dermokine-regulated phosphorylated sites, we counted the number of sites on each phosphorylated protein belonging to the pathways associated with “cadherin binding” and “adherens junctions” associated to clusters 2, 4, 5 and 7. We found several phosphorylated sites (between 8 and 12) on proteins associated to cell-cell adhesion, including on the TNKS1BP1 (12), TJP1 (11), SCRIB (10), TJP2 (10), CTNNB1 (9), AFDN (8) and CTNND1 (or p120) (8) (Supplemental Figure 6 and Supplemental Table 5). Among these proteins, p120 was phosphorylated on S252, S268, S288 and T916, all sites playing crucial roles in modulating cell-cell adhesion complexes and cytoskeletal dynamics(23, 43, 44). To confirm that the regulated

phosphorylated sites identified on p120 as well as other proteins were bona-fide phosphorylated sites due to changes in kinase activity and independent of alterations in protein abundance (45), we normalized the phosphoproteome on the proteome (Supplemental Figure 7A). We found that the normalized phosphoproteome of WT differed from that of *DMKN* βγ-/- and *DMKN* αβ-/- keratinocytes. When the *DMKN* βγ-/- and *DMKN* αβ-/- keratinocytes were treated with recombinant dermokine, their phosphoproteome became similar to the phosphoproteome of WT keratinocytes (Supplemental Figure 7A). This finding is consistent with the result observed before normalization (Figure 5A-B). The phosphorylation pattern on p120 also remained unchanged after normalization (Supplemental Table 4). We validated the phosphorylation of p120 on two of the identified phosphorylated sites, serine 252 (S252) and serine 268 (S268), for which antibodies and fully annotated MS/MS spectra were available (Supplemental Figure 7B-C). Immunoblot analysis of lysates from *DMKN* βγ-/-, *DMKN* αβ-/- and WT keratinocytes showed that the phosphorylation of both S252 and S268 on p120 increased in the absence of dermokine (Supplemental Figure 7D). Furthermore, we observed that p120 phosphorylation was similar to WT when recombinant dermokine was added to *DMKN* βγ-/-, *DMKN* αβ-/- and WT keratinocytes (Supplemental Figure 7E). In summary, the phosphoproteomics analyses of dermokine KO samples identified differentially phosphorylated proteins, including p120.

Dermokine regulates cell-cell adhesion in keratinocytes

As p120 is known to regulate cell-cell adhesion (44) and “cell-cell adhesion” was also one of the dysregulated GO terms in the proteomics and phosphoproteomics analysis of the KO samples (Figure 4C, Supplemental Figure 4 and Supplemental Table 5), we next tested whether dermokine regulates cell-cell adhesion of keratinocytes using two different cell-cell adhesion assays (46, 47). An EDTA-based cell-cell adhesion assay showed that dermokine-ablated keratinocytes had significantly fewer cell clusters containing more than four cells compared to WT keratinocytes after EDTA treatment (Figure 5A and Supplemental Figure 8A). This finding suggests impaired cell-cell adhesion in dermokine depleted cells. To further test this possibility, we performed a dispase dissociation assay using independent *DMKN* βγ-/-, *DMKN* αβ-/- and *DMKN* αβγ-/- clones(47), and found an increase in the fragmentation of all the KO cells after dispase treatment (Figure 5B). These results confirm the impaired cell-cell adhesion in the KO cells, regardless of dermokine isoforms and clones. As we did not observe a change in cadherin-1 (CDH1) abundance by proteomic analysis of 2D cultures and IHC staining of WT, *DMKN* βγ-/-and *DMKN* αβ-/- 3D organotypic skin cultures (Figure 3A-B and Supplemental Figure 8B-C), we tested whether p120 may be involved in the dermokine-mediated effect on

cell-cell adhesion in keratinocytes. Therefore, we performed the same cell-cell adhesion assays in keratinocytes depleted of p120 by small interfering RNA (siRNA). The efficient knock-down was confirmed by immunoblotting (Supplemental Figure 8D). As previously shown (44), knock-down of p120 significantly decreased cell-cell adhesion in WT cells (Figure 5C and Supplemental Figure 8E-G). Surprisingly, however, depletion of p120 in *DMKN* αβ-/- and *DMKN* βγ-/- keratinocytes decreased fragmentation in the dispase dissociation assay and increased the number of cell clusters containing more than four cells in the EDTA-based cell-cell adhesion assay, reaching values similar to WT cells (Figure 5C and Supplemental Figure 8E-H). These findings suggest that the increased phosphorylation of p120 observed in KO cells (Supplemental Figure 7D-E) may have a negative effect on the adhesive properties of p120 downstream of dermokine, confirming observations in other model systems (23, 48, 49). To test this idea, we generated siRNA resistant mutants of p120 where S252 and S268 were substituted by aspartic acid (D) (S252D, S268D) to mimic constitutive phosphorylation (Supplemental Figure 8I) and used them in the dispase dissociation assay. We confirmed that p120 depletion reduced fragmentation in KO keratinocytes (Figure 5C-D). Most importantly, upon expression of the two phosphomimetic p120 mutants in p120 knock-down cells, the fragmentation in KO keratinocytes returned to the level seen in unperturbed KO cells (Figure 5D). This data suggest that dermokine modulates cell-cell adhesion, at least in part, through p120 phosphorylation. Together, our data demonstrate that dermokine regulates cell-cell adhesion in keratinocytes, possibly by affecting phosphorylation of p120.

Dermokine is a regulator of ROCK signaling

To gain insight into the molecular mechanisms underlying the dermokine-p120 interplay, we transfected WT and dermokine KO keratinocytes with p120 or control siRNA and analyzed changes in the proteome. Using HRMS1-DIA, we identified 101288 precursors, 78704 peptides, and 7394 proteins across all conditions, with high Pearson correlations between biological replicates (Supplemental Figure 9A-B, Supplemental Table 6). Hierarchical clustering of differentially abundant proteins revealed four clusters with distinct abundance patterns (Figure 6A). For instance, Cluster 1 contained proteins whose abundance decreased upon p120 perturbation, including p120 itself and proteins regulating cell adhesion, such as α- and β-catenin and cadherin (Figure 6A-B. Supplemental Table 7). Interestingly, Cluster 4 included proteins whose abundance followed the pattern observed in the dispase and wound closure assays (Figures 5, and 6A-B). Pathway enrichment analysis across clusters highlighted overhead terms associated with RhoA signaling, signal transduction, transport, and adherens junction (Figure 6C, Supplemental Figure 9C, and Supplemental Table 8). Specifically,

Cluster 4 was enriched for RhoA-associated proteins, like Cluster 1, suggesting that p120-perturbed KO cells and WT unperturbed keratinocytes shared similar levels of proteins associated with Rho signaling (Figure 6C, Supplemental Figure 9C, and Supplemental Table 8). These findings align with the results of the KSEA of phosphoproteomics data, which indicated significantly higher activity score of ROCK1 in KO cells relative to WT keratinocytes (Figure 3B and Supplemental Table 5). Based on these data, we hypothesized that RhoA signaling and its target ROCK1 (50) modulate the adhesion phenotype downstream of p120 in dermokine KO cells. We functionally tested this possibility using the ROCK inhibitor (ROCKi) Y-27632–in dispase assays (Figure 6D). In WT and KO cells transfected with control siRNA, we did not observe a difference between ROCKi- and DMSO-treated cells (Figure 6D). Upon p120 knock-down, both WT cells and KO cells showed significantly more fragments relative to unperturbed cells when we normalized ROCKi- to DMSO-treated cells (Figure 6D). Furthermore, the number of fragments, indicating the extent of adhesion, was higher in KO than in WT cells in the latter conditions (Figure 6D). Together with data presented in Figure 5, these findings support the idea that, upon dermokine ablation, the p120-dependent adhesion phenotype is more sensitive to ROCK1 inhibition than in p120 perturbed cells alone.

Taken together, this data points to ROCK1 as a regulator of cellular adhesion downstream of the dermokine-p120 system in keratinocytes.

Dermokine expression is reduced in the hyperthickened epidermis of non-healing wounds

As abnormal dermokine expression has been previously associated with skin disorders (51), we stained skin biopsies from healthy and psoriatic skin, poorly- and well-differentiated SCCs as well as non-healing wounds (venous leg ulcers), for dermokine and p120 (Figure 7, Supplemental Figure 10, and Supplemental Table 9). We observed dermokine expression in suprabasal keratinocytes of healthy skin, psoriasis, poorly- and well-differentiated SCCs (Supplemental Figure 10A-C), but a much weaker staining intensity in the hyperthickened epidermis of non-healing wounds (Figure 7A-B and Supplemental Figure 10D). We quantified dermokine expression relative to the distance to the wound bed in chronic wounds and found that keratinocytes proximal to the wound edge showed significantly lower dermokine expression across the epidermal profile, whereas, within the same biopsy, keratinocytes further away from the wound showed no change in dermokine expression (Figure 7C and Supplemental Figure 10E). To visualize the distance that keratinocytes express dermokine relative to the wounded tissue, we fitted a non-linear regression curve previously used to explain differences

in patient data from non-healing wounds and healthy skin(52). This analysis revealed that the average rate (K(Fast)) at which dermokine expression decreases, was higher in non-healing wound-edge keratinocytes (K(Fast) = 4.4E-03) compared to wound-edge distal keratinocytes in the respective biopsies (K(Fast) = 5.7E-08) (Figure 7C). Therefore, our data show less dermokine expression only in keratinocytes adjacent to the wound bed, which is consistent with the impaired differentiation of suprabasal keratinocytes in such wounds. Next, we evaluated changes in total and phosphorylated p120. For the latter, we used antibodies against phosphorylated S252 to recapitulate the immunoblotting findings and against phosphorylated T310 quantified in the phosphoproteomics dataset (Supplemental Figure 7D-E), Supplemental Table 4). After normalization of phosphorylated over total levels of p120 we found a significant increase in S252- and T310-phosphorylated p120 in non-healing wounds compared to healthy skin (Figure 7D-F and Supplemental Figure 10F).

In conclusion, as all the tested phosphorylated sites on p120 are known to inhibit cell-cell adhesion (23, 48, 49), our results demonstrate that reduction of dermokine expression correlates with increased p120 phosphorylation, suggesting that the results obtained in vitro are also relevant for diseased skin in vivo (Figure 8).

Discussion

This study combines genome engineering, multi-proteomics analyses of 2D keratinocyte monocultures and 3D organotypic cultures, and staining of patient-derived samples to elucidate the function of dermokine in keratinocytes. Unlike earlier studies, which relied on mRNA quantification to distinguish isoforms (14), we quantified domain-specific proteotypic peptides via targeted proteomics and suggest an alternative to immunoblotting for validation of protein ablations (53). The dermokine locus encodes multiple transcripts generated via alternative splicing or promoter usage, resulting in isoforms with distinct expression patterns. While dermokine-β and -γ are highly expressed in differentiating keratinocytes, dermokine-α mRNA was detected in all epidermal layers and in the placenta(17). Genetic ablation of dermokine-βγ in mice had no effect on cutaneous wound healing but led to transient defects in cornification after birth (13). However, the expression of dermokine-α is strongly increased in the skin of these animals, potentially compensating for the loss of other isoforms. This is important, because dermokine-α has a 77.27% homology to the C-terminal domain of dermokine-β, yet it is regulated via a distinct promoter (17). Interestingly, our data revealed no major functional differences between dermokine isoforms in cultured human keratinocytes, suggesting functional overlap. The difference to the mouse data may be explained by differences in murine versus human keratinocytes. Consistent with this possibility, murine and human skin differ in epidermal thickness, hair follicle density and keratinocyte biomechanics (50, 52). Alternatively, factors that are present in vivo, but not in vitro, may affect the function of different dermokine isoforms. A major advantage of our system is the focus on direct effects of dermokine on keratinocytes, because of the lack of vasculature and immune cells. However, effects of such cells on dermokine function should be determined in future studies, for example after transplantation of the 3D skin equivalents onto immunodeficient mice.

Dermokine, along with SBSN and KRTDAP, is part of the SSCexpressed in suprabasal layers of the stratified epidermis (34). These genes are grouped in the same genomic locus and are transcribed in the same direction during epidermal development (34). Our data show that the dermokine knockout reduced the abundance of SBSN and KRTDAP, both known to be expressed during the late differentiation state of keratinocytes (34), as well as filaggrin, another late-stage differentiation marker (54). Therefore, dermokine regulates the abundance of several late-stage keratinocyte differentiation proteins essential for epidermal homeostasis, most likely through effects on keratinocyte differentiation. To uncover the function of dermokine in keratinocytes, we performed phosphoproteomics of *DMKN* αβ-/-, *DMKN* βγ-/- and WT keratinocytes using optimized DIA assays,

combined with semi-automated phosphorylated peptide enrichment, which allowed us to substantially reduce our input material from commonly used 3-5 mg to 200 µg lysate (38). Despite the relatively low amount of starting material, we could fully quantify almost 5000 phosphorylated sites. This workflow will benefit other research groups, who are limited by the amount of biological material, e.g. when using FFPE tissues or single cells (55, 56). Click or tap here to enter text.Using this approach, we identified increased phosphorylation of p120 in dermokine-depleted keratinocytes. Technological developments, including the de novo sequencing tool (57) might uncover other phosphorylation sites. Functionally, impaired adhesion of dermokine-depleted keratinocytes was rescued by p120 knock-down, whereas expression of a phosphomimetic p120 mutant failed to restore confirming previous observations of a negative effect of p120 phosphorylation on adhesion (23, 43, 44). It is possible that phosphorylated p120 has a shorter half-life compared to the non-phosphorylated form and that the knock-down mainly affects the phosphorylated form within the experimental time frame. Our data point to a direct role of p120 phosphorylation in dermokine-dependent regulation of cell-cell adhesion both in vitro and in vivo (23, 43, 44). Although, the role of p120 phosphorylation in regulating cell-cell adhesion remains controversial, Mendonsa et al. (23) showed that the phosphorylation state of p120 plays a role in the control of cadherin-1. By converting p120 serine/threonine sites (including T310 and S252) to alanine, cell-cell adhesion was strengthened via cadherin-1-mediated binding in breast cancer cells. A possible underlying mechanism might be that the p120-armadillo-repeat region, shortly after phosphorylated T310, may bind to the cadherin-1 juxtamembrane domain (23). Conceivably, the increased p120 phosphorylation in the absence of dermokine may inhibit the binding of p120 to cadherin-1 by steric hindrances and induce protein turnover by internalization of cadherin-1 via endocytosis (44). However, unchanged cadherin-1 observed by proteomics and staining of 3D organotypic cultures suggests that cadherin-1 remains present at the cell surface of the dermokine knockout cells, although its function may be affected. Our phosphomimetic and loss-of-function data identify p120 as a regulator of dermokine-dependent adhesion. Our data are consistent with prior work showing that phosphorylation of p120 on serine and threonine residues modulates adhesion (42, 58). We suggest a model in which p120 phosphorylation weakens keratinocyte adhesion by modulating Rho family kinases and downstream cytoskeletal rearrangement (59). Furthermore, we suggest that dermokine regulates signaling proteins, such as SRC, to modulate p120 phosphorylation which in turn influences ROCK1 activity. Our phosphoproteomic data suggests that SRC, casein kinase 1 epsilon (CSNK1E), and ERK1/ERK2, which are known to phosphorylate p120 at Y228, S268, T310, respectively (23, 43, 60, 61) may be responsible for

388 the dermokine-p120-cadherin-1-dependent phenotype. This hypothesis remains to be tested in future studies.
389 Taken together, our phosphoproteomics and functional assays generate in vivo predictions, that can be
390 addressed in vivo once mice with keratinocyte-specific dermokine knockout will be available.

391 Previous research investigating dermokine expression in human skin disorders has utilized an in-house anti-
392 dermokine-βγ antibody and provided qualitative information (51). Here, we used a commercially available anti-
393 dermokine-β and a putative dermokine-γ antibody (62) and quantified stainings in healthy and diseased human
394 samples. Dermokine levels remained unchanged in healthy skin, psoriasis and all SCCs, while non-healing
395 wounds showed the strongest changes. Contrary to our findings, Hasegawa *et al.* showed reduced dermokine
396 expression in poorly differentiated SCCs and increased dermokine expression in both psoriatic skin and acute
397 wounds (51). A possible explanation for the different wound healing data might be that we stained non-healing
398 human wounds (venous leg ulcers), while Hasegawa *et al.* used an acute murine wound healing model (51).
399 Therefore, either species-specific differences or differences between acute and chronic wounds may account
400 for these different findings. Keratinocytes at the edge of non-healing wounds fail to differentiate properly and
401 show reduced adhesion (6, 63, 64). While dermokine expression decreased in non-healing wounds,
402 phosphorylated p120 increased relative to healthy skin. Together with our in vitro data, these findings suggest
403 that keratinocyte adhesion is impaired in chronic ulcers, consistent with previous studies reporting that certain
404 cell-cell adhesion proteins are downregulated in venous leg ulcers (6). Further studies are necessary to
405 establish whether impaired dermokine expression directly contributes to certain aspects of the chronic wound
406 phenotype.

407 The functional multi-omics approach used in this study improves our understanding of dermokine function and
408 p120 phosphorylation in non-healing wounds. Our data show low dermokine expression and high p120
409 phosphorylation in non-healing wounds linking dermokine with cell-cell adhesion. Consistent with this, our 3D
410 organotypic model provided cell-autonomous evidence for dermokine in keratinocytes without confounding
411 species-specific or immunological effects. More broadly, our approach might guide drug development for
412 cutaneous biology when integrating “-omics” techniques with functional assays (65).

413

Materials and Methods

Sex as a biological variable

Our study examined male and female patients, and similar findings are reported for both sexes. The N/TERT-1 keratinocyte cell line used for this study is of male origin and commercially available human dermal fibroblasts are derived from male and female donors. However, sex as a biological variable was not considered in this study.

Cell culture

Human keratinocyte telomerase reverse transcriptase immortalized (h/TERT immortalized) N/TERT-1 cells are derived from clinically normal foreskin tissue (gift from Prof. Dr. Edel O'Toole, Queen Mary University, London,UK). N/TERT-1 keratinocytes were grown in DMEM/F12 growth medium ((DMEM/F-12 (Thermo Fisher Scientific), 10% fetal bovine serum (FBS) (Thermo Fisher Scientific), 1% penicillin/streptomycin (P/S) (Sigma-Aldrich)) supplemented with RM+ (DMEM/F-12 (Thermo Fisher Scientific), 10% fetal bovine serum (FBS) (Thermo Fisher Scientific), 1% penicillin/streptomycin (P/S) (Sigma-Aldrich), 0.4 µg/mL hydrocortisone (Sigma-Aldrich), 0.5 µg/mL insulin (Sigma-Aldrich), 10 ng/mL epidermal growth factor (BioRad), 0.1 nM cholera toxin (Sigma-Aldrich), 5 µg/mL transferrin (Sigma-Aldrich), 20 pM liothyronine (Sigma-Aldrich)) in a humidified incubator at 37°C and 5% CO2. Commercially available human dermal fibroblasts were purchased from Sigma-Aldrich (Sigma-Aldrich) and grown in DMEM (Thermo Fisher Scientific), 10% FBS (Thermo Fisher Scientific) and 1% P/S (Sigma-Aldrich). All cell lines were tested mycoplasma negative before transfection using a commercial kit (Sigma-Aldrich). Keratinocytes were regularly tested for differentiation status using anti-keratin 14 (1:1000, #ab7800) and anti-keratin-10 (1:150, #ab76318) antibodies, as previously published (66).

Calcium-dependent keratinocyte assay

75.000 N/TERT keratinocytes were seeded into a coated 8 well chamber coverslip (Ibidi; # 80806) and incubated for 24 hours. Cells were briefly washed with trypsin-EDTA (Sigma-Aldrich; #T3924) and incubated 24 h in full growth DMEM/F12 containing either 1 mM calcium- or 5 mM calcium. Cells were fixed with 4 % PFA for 15 min, washed with PBS permeabilized with 0.5 % Triton-X 100 (Merck, X100-100ML) for 10 min and blocked in 5 % BSA in PBS for 60 min at RT. Cells were incubated overnight with primary antibodies, anti-keratin 14 (0,1 µg/mL; Abcam, #ab7800) and anti-keratin-10 (1:150; Abcam, #ab76318) at 4°C. After three PBS washes secondary antibodies, anti-mouse Alexa Fluor 488 (1 µg/mL; Invitrogen, #A11001) and anti-

rabbit Alexa Fluor 568 (2 µg/mL; Invitrogen, #A11011) were added for 1 h at RT. Nuclei were counterstained with DAPI (4',6-Diamidino-2-Phenylindole, Dihydrochloride; Thermo Fisher Scientific; #D1306) for 10 min , followed by washing and mounting (Thermo Fisher Scientific; #9990402). Cover slips were kept in dark until imaging. Images were acquired with a Leica DMIL LED Fluo microscope. Three images perreplicate were analyzed using Leica LAS X software (Version 3.8.2.27713). Positively stained areas were automatically determined and average intensity of stained area was reported. Statistical analysis was performed in GraphPad Prism (Dotmatics using an unpaired t-test.

Guide RNA design

Guide RNAs (gRNAs) were designed utilizing the general settings of the CHOPCHOP web tool to target specific sequences associated with the isoforms of the dermokine gene.

For the chemical-transfection approach we used gRNA 1, targeting exon 2. For the Atomic-Force-Microscopy (AFM) based approach we used a Cas9 strategy to delete exon 18.

Chemical transfection to generate *DMKN* βγ-/- keratinocytes

Gene editing was performed using a two-plasmid system enabling intracellular assembly of Cas9 and DMKN-targeting gRNA (GGATACCCCGGAAACTCAGC).. The Cas9 expression plasmid (CAS9PBKS; Addgene), encoded linked to GFP) via a 2A peptide (Cas9-2A-GFP). The gRNA expression plasmid was reconstructed by cloning *DMKN*-targeting gRNAs (Macrogen) into the U6GRNA (Addgene) vector. To vector was linearized with Bbs1, and annealed oligos were annealed using T4 ligase (New England Biolabs). Following ampicillin selection in *E. Coli*, successful insertion was confirmed by Sanger sequencing (Macrogen). Keratinocytes were seeded at 500.000 cells/mL in 6 well-plates one day prior to transfection, to achieve 50-80% confluency. For each transfection, 1 µg of CAS9PBKS plasmid and 1 ug of gRNA plasmid were combined in 200 µL JetOPTIMUS® buffer with of 2 µL JetOPTIMUS® reagent, incubated at RT for 10 min and applied to keratinocytes. Two days post- transfection, GFP-positive cells were sorted by flow cytometry using an MA900 cell sorter (Sony Biotechnology), with non-transfected keratinocytes used to define gating. The GFPhigh (top 10-15%) population was collected, cultured for 2 weeks and single-cell sorted into 96-well plates. Genomic DNA was extracted from 10.000 cells using QuickExtract™ DNA extraction solution (LGC Biosearch Technologies). Cells were washed with PBS, resuspended in 30-50 µL of QuickExtract™ DNA extraction solution, incubated at 70°C for 20 min and heated to 95°C for 10 min. PCR was performed PROFILase™ 2x

Master Mix (COBO Technologies) with the following primers: forward TCATTCTGGTTGCTGGCTCT and reverse TCTACCAGGGTCAGAGATGGT. Amplification was carried out on an ABI Veriti™ thermocycler (Thermo Fisher Scientific). PCR products were purified with ExoSAP-IT™ and submitted to Macrogen for Sanger sequencing. Editing efficiency and genotype composition were analyzed using the Synthego ICE tool.

FluidFM™ based nano-injection to generate *DMKN* αβ-/- keratinocytes

The principle of FluidFM™ hase been described previously (24) , including its use formultiplex editing in CHO-K1 cells (27). Single keratinocytes were seeded into the center of a well of 12-well plates using a DispenCell™ (SEED Biosciences) and allowed to adhere overnight. 50-100 fL of RNP solution was injected into the nucleus of single cells using FluidFM™. The injection mixture contained 0.5 pmol gRNA (TCATCACTGCAGAAACGTGC; IDT), 0.366 pmol Cas9 *(*IDT*)* and 20 ng/µL GFP mRNA (Milteny). Injection Successful injcetions were monitored 24 h later by fluorescent microscopy. Single cells were clonally expanded. To improve outgrowth, untreated keratinocytes were seeded into co-culture inserts within the same wells. When colonies reached 1.000 cells, cultures were rinsed with PBS,, briefly incubated (3 min) in PBS/0.001M EDTA, detached with TrypLE (15min; ThermoFischer), resuspended and re-seeded into the same well. After 48-72 h, cells were detached and split at a 1:3 ratio into a 12-well plate. A third of the cells were collected genomic DNA isolation using QuickExtract (Lucigen). PCR amplification was performed using the PlatinumTaq DNA polymerase and GC enhancer (Thermo Fisher Scientific) 1 µL of DNA lysate under the following conditions: 1) 95°C, 240 s, 2) 95°C, 30 s, 3) 67.1°C, 30 s, 4) 72°C, 45 s, steps 2-4 were repeated 35x). Primers (0.4 µM each) were: forward: ACGGTCCAAGTGGAGAAGCCGT*,* and reverse: tcctGCCCTCAAGACCTCTGCC. PCR products were analyzed on 1.5% (w/v) agarose/TAE gels at 100 V for 25 min alongside a 100 bp ladder (GeneRuler). For Sanger sequencing, : 7.5 µL of PCR product (50-300 ng) was purified using ExoSAPIT™ (Thermo Fisher Scientific), adjusted to 12 µL with ultra-pure water, mixed with 3 µL of forward primer (20 µM) and submitted to Microsynth™ for sequencing.

Analysis of CRISPR/Cas9 mediated genome engineering

N/TERT-1 human keratinocytes edited by eitherFluidFM™ or chemical transfection were validated by Sanger sequencing as described above. Trace files were aligned to the ENSEMBLE target sequence using Benchling™ and chromatograms complementary to the gRNA were inspected for overlapping peaks or deletions indicative of indel formation.Sequencing files from selected clones were deconvoluted using

INDIGO™ (Gear Genomics) and individual allele sequences were aligned to the control sequence to visualize the deletions or insertions. Clones carrying frame-shift mutations (indels not dividable by 3) in all alleles were considered knockouts (Supplemental Figure 1).

Generation of human *DMKN* αβ-/- and *DMKN* βγ-/- keratinocyte 3D organotypic skin cultures

3D organotypic skin cultures were generated by placing 600 µL of collagen/Matrigel (Corning) matrix containing 100.000 human dermal fibroblasts (Sigma-Aldrich) (210 µL collagen I (Corning), 210 µL Matrigel (Corning), 59 µL 10x MEM (Thermo Fisher Scientific), 59 µL FBS (Thermo Fisher Scientific), and 59 µL fibroblasts (Sigma-Aldrich)) into a new 12-well plate Transwell insert (Sigma-Aldrich). After polymerization for 1 h at 37°C, 59 µL of either WT, *DMKN* αβ-/- or *DMKN* βγ-/- keratinocytes (1.000.000 cells), were seeded onto the matrix and RM+ media was added below the insert. After overnight incubation at 37°C, cultures were airlifted and grown at the air-liquid interface for 15 days with daily medium changes. After 15 days, the 3D cultures were cut in half: one half was fixed in 4% PFA (Sigma-Aldrich) for 30 min at RT and paraffin-embedded for IHC analysis .The other half was snap-frozen in liquid nitrogen for proteomics analysis.

Hematoxylin/eosin and immunohistochemical staining of WT, *DMKN* αβ-/- and *DMKN* βγ-/- 3D organotypic skin cultures

DMKN KO and WT 3D organotypic skin culture sections were stained with hematoxylin (Sigma-Aldrich) for 5 min, washed in tap water for 5 min followed by eosin (Sigma-Aldrich) for 5 and another 5 min tap water wash. Sections were dehydrated with 96% and 99% ethanol (Sigma-Aldrich), air-dried and mounted with Pertex (Histoline).

Paraffin sections (4 µm; Shandon microtome) were dried overnight at 35°C. IHC staining followed the manufacturer's instructions (Thermo Fisher Scientific). Sections were heated at 60°C for 60 min, deparaffinized, rehydrated and blocked with Ultra V Block (Thermo Fisher Scientific) for 5 min. Slides incubated with anti-dermokine antibody (1:100; Abcam) were directly treated for 1 h and rinsed with TBS (Sigma-Aldrich). Slides stained with anti-Ki-67 (1:200; Abcam) or anti-ITGα6 (1:500; Abcam) were pre-treated in EDTA buffer (10 mM Tris,1 mM EDTA, pH 9.0). Slides stained with anti-cadherin-1 (1:50; BD Biosciences), anti-KRT10 (1:1000; Abcam) or anti-KRT14 (1:500; Abcam) antibodies were pre-treated in citrate buffer (100 mM citric acid,100 mM sodium-citrate, pH 6.0). All slides were boiled in EDTA or citrate buffer for 15 min, cooled for 15 min and washed twice.

Primary antibody enhancer (Thermo Fisher Scientific) was applied for 10 min followed by three 5 min washes. HRP Polymer (Thermo Fisher Scientific) was applied for 15 min and washed similarly. Slides were developed with DAB (Thermo Fisher Scientific) for 10 min,washed and stained with hematoxylin (Sigma-Aldrich) for 15 s, rinsed for 5 min and mounted in Pertex (Histoline). The images were on an EVOS M5000 (20x magnification; Thermo Fisher Scientific).

Semi-quantitative IHC analysis was performed in QuPath. Entire epidermal-like regions were drawn manually, DAB signal intensities were quantified using a pixel-based thresholder and values were visualized in GraphPad Prism (Dotmatics).

Immunofluorescence and quantification of patient tissue

FFPE tissue samples from healthy skin, SCCs, wounds and psoriasis were selected and retrieved from the SKINTEGRITY.CH biobank of the Department of Dermatology, University Hospital Zurich. The blocks were used to prepare 7 µm tissue sections and stained. Patient information is available in original data file.

FFPE sections were dried for 30-60 min at 60°C before being dewaxed, rehydrated, and PBS-buffered. Antigen retrieval was performed with 0.1 M sodium citrate buffer (pH 6) for 45 minutes at 95°C. After three washes with PBST (PBS + 0.1% Tween), unspecific binding to tissue sections was blocked for 1 h at RT with 12% BSA in PBST. Primary antibody was diluted (catenin δ-1 (Cell Signaling Technology) (1:200), dermokine (Abcam) (1:250), phospho-catenin δ-1 Thr310 (Abcam) (1:250) and phospho-catenin δ-1 Ser252 (Cell Signaling Technology) (1:250)) in blocking buffer and incubated overnight at 4°C. Following three washes, slides were incubated for 1 h at RT with the secondary antibody (anti-rabbit-IgG-Cy3, 1:200) and 1 µg/ml Hoechst 33342 (Sigma-Aldrich) in blocking buffer. Following another three washes, sections were mounted using Mowiol with DABCO®. Slides were scanned with an Axioscan 7 slide scanner (Carl Zeiss AG).

Staining intensity was quantified using Qupath (version 0.5.0). Positively stained area was determined using a pixel thresholder and median intensity of stained area was reported. Data were analyzed in GraphPad Prism (Dotmatics).

Statistics

All experiments were repeated at least three times as independent biological replicates with similar results. Representative Western blots or IF or IHC images are shown. The number of independent experiments,

treatments and relative controls and statistical analysis are indicated in Figure legends. $P < 0.05$ was considered significant. *P* values were calculated using a 2-tailed Student's *t* test. One- or two-way ANOVA was used with post-hoc tests as indicated in the figure legends.

Study approval

All patient-derived samples used were surplus material from routine surgeries and were provided by the Dermatology Department of the University Hospital Zürich, Switzerland, with the assistance of the SKINTEGRITY.CH biobank. The surplus biopsies stored in the biobank were from consenting patients. The use of material for research purposes was approved by the local ethics commissions (Cantonal Ethic Commission Zürich: project no. 2017-00684). All experiments conformed to the principles set out in the World Medical Association's Declaration of Helsinki and the Department of Health and Human Services Belmont Report. All human cell line experiments were performed with the approval of the Technical University of Denmark.

Data availability

The mass spectrometry proteomics data have been deposited to the ProteomeXchange Consortium through the PRIDE partner repository with the following accession codes: PXD050151, PXD055812 and PXD074943. The targeted proteomics data have been uploaded to the Panorama repository, available via the Panorama Public doi: doi.org/10.6069/hgvx-qe48.

This paper reports original code: (https://github.com/VahapCan/Dermokine_Analysis_Canbay_2024).

Underlying data points are available in the Supporting data values document.

Funding support

Wellcome Trust (107636/ Z/15/Z and 107636/Z/15/A) to C.F.

Novo Nordisk Foundation Young Investigator Award (call 2022, NNF22OC0070845) to C.F.

Novo Nordisk Foundation Young Investigator Award (call 2016, NNF16OC0020670) to U.a.d.K.

LEO Foundation (LF-OC-23-001220) to C.F.

LEO Foundation (LF-OC-19-000033) to U.a.d.K.

Acknowledgements

The authors would like to thank Prof. Dr. Sabine Werner for her continuous support, especially after U.a.d.K.'s sudden passing, and for reading the manuscript. Mass-spectrometry analysis was performed at the Proteomics Core, Technical University of Denmark, and the Metabolomics and Proteomics Platform at the University of Fribourg. We thank M. Wennekers Nielsen, M. Vestergaard Lukassen, and Dr. K. Kalogeropoulos (Technical University of Denmark). Human n/TERT keratinocytes were a kind gift from Prof. Dr. Edel O'Toole. J.H., J.D. and U.a.d.K are/were members of the SKINTEGRITY.CH interdisciplinary research consortium. We thank the patients for donation of biopsies.

Conflict of interest

T.A.B., A.M.H and S.M. are employees of Cytosurge AG. T.A.B. owns shares in Cytosurge AG.

Author Contributions

U.a.d.K. conceived the project and acquired funding, now administered by C.F.. U.a.d.K., C.F., J.D. and V.C. designed the experiments. V.C., T.W., W.T., T.A.B., A.M.H., S.M., C.C., M.S. and C.R.E. performed the experiments. C.F. and V.C. wrote the manuscript. All authors read, revised and approved the manuscript.

References

1. Candi E, Schmidt R, Melino G. The cornified envelope: a model of cell death in the skin. Nature Reviews Molecular Cell Biology 2005 6:4. 2005;6(4):328–340.

2. Murata T, et al. Stratum corneum as polymer sheet: concept and cornification processes. Trends Mol Med. 2022;28(5):350–359.

3. Cangkrama M, Wietecha M, Werner S. Wound Repair, Scar Formation, and Cancer: Converging on Activin. Trends Mol Med. 2020;26(12):1107–1117.

4. Hodorogea A, et al. Epithelial-Mesenchymal Transition in Skin Cancers: A Review. Analytical Cellular Pathology. 2019;2019:1–11.

5. Afonina IS, Van Nuffel E, Beyaert R. Immune responses and therapeutic options in psoriasis. Cellular and Molecular Life Sciences. 2021;78(6):2709–2727.

6. Stojadinovic O, et al. Deregulation of keratinocyte differentiation and activation: a hallmark of venous ulcers. J Cell Mol Med. 2008;12(6b):2675–2690.

7. Xie Z, et al. p120-catenin is required for regulating epidermal proliferation, differentiation, and barrier function. J Cell Physiol. 2019;234(1):427–432.

8. Menke NB, et al. Impaired wound healing. Clin Dermatol. 2007;25(1):19–25.

9. de Veer SJ, et al. Proteases: Common culprits in human skin disorders [preprint]. Trends Mol Med. 2014;20(3):166–178.

10. Pondeljak N, et al. Key Factors in the Complex and Coordinated Network of Skin Keratinization: Their Significance and Involvement in Common Skin Conditions. Int J Mol Sci. 2023;25(1):236.

11. Krampert M, et al. Activities of the matrix metalloproteinase stromelysin-2 (MMP-10) in matrix degradation and keratinocyte organization in wounded skin. Mol Biol Cell. 2004;15(12):5242–5254.

12. Schlage P, et al. Matrix Metalloproteinase 10 Degradomics in Keratinocytes and Epidermal Tissue Identifies Bioactive Substrates With Pleiotropic Functions. Mol Cell Proteomics. 2015;14(12):3234–3246.

13. Leclerc EA, et al. Mice deficient for the epidermal dermokine β and γ isoforms display transient cornification defects. J Cell Sci. 2014;127(13):2862–2872.

14. Utsunomiya A, et al. Homeostatic Function of Dermokine in the Skin Barrier and Inflammation. Journal of Investigative Dermatology. 2020.

15. Pasparakis M, Haase I, Nestle FO. Mechanisms regulating skin immunity and inflammation. Nat Rev Immunol. 2014;14(5):289–301.

16. Kumari S, Pasparakis M. Epithelial Cell Death and Inflammation in Skin. Curr Top Microbiol Immunol. 2017;403:77–93.

17. Naso MF, et al. Dermokine: an extensively differentially spliced gene expressed in epithelial cells. J Invest Dermatol. 2007;127(7):1622–1631.

18. Toulza E, et al. The human dermokine gene: description of novel isoforms with different tissue-specific expression and subcellular location. J Invest Dermatol. 2006;126(2):503–506.

19. Enjalbert F, et al. 3D model of harlequin ichthyosis reveals inflammatory therapeutic targets. Journal of Clinical Investigation. 2020;130(9):4798–4810.

20. Smits JPH, et al. Immortalized N/TERT keratinocytes as an alternative cell source in 3D human epidermal models. Sci Rep. 2017;7(1):11838.

21. McGeoghan F, et al. RNA sequencing and lipidomics uncovers novel pathomechanisms in recessive X-linked ichthyosis. Front Mol Biosci. 2023;10.

22. Berning M, et al. Three-Dimensional In Vitro Skin and Skin Cancer Models Based on Human Fibroblast-Derived Matrix. Tissue Eng Part C Methods. 2015;21(9):958–970.

23. Mendonsa AM, Bandyopadhyay C, Gumbiner BM. p120-catenin phosphorylation status alters E-cadherin mediated cell adhesion and ability of tumor cells to metastasize. PLoS One. 2020;15(6):e0235337.

24. Meister A, et al. FluidFM: Combining Atomic Force Microscopy and Nanofluidics in a Universal Liquid Delivery System for Single Cell Applications and Beyond. Nano Lett. 2009;9(6):2501–2507.

25. Dickson MA, et al. Human keratinocytes that express hTERT and also bypass a p16(INK4a)-enforced mechanism that limits life span become immortal yet retain normal growth and differentiation characteristics. Mol Cell Biol. 2000;20(4):1436–1447.

26. Lonowski LA, et al. Genome editing using FACS enrichment of nuclease-expressing cells and indel detection by amplicon analysis. Nat Protoc. 2017;12(3):581–603.

27. Antony JS, et al. Accelerated generation of gene-engineered monoclonal CHO cell lines using FluidFM nanoinjection and CRISPR/Cas9. Biotechnol J. 2024;19(4).

28. Sanger F, Coulson AR. A rapid method for determining sequences in DNA by primed synthesis with DNA polymerase. J Mol Biol. 1975;94(3):441–448.

29. Picotti P, Aebersold R. Selected reaction monitoring–based proteomics: workflows, potential, pitfalls and future directions. Nat Methods. 2012;9(6):555–566.

30. Canbay V, auf dem Keller U. New strategies to identify protease substrates. Curr Opin Chem Biol. 2021;60:89–96.

31. Watt FM. NEW EMBO MEMBER'S REVIEW: Role of integrins in regulating epidermal adhesion, growth and differentiation. EMBO J. 2002;21(15):3919–3926.

32. Francavilla C, et al. Functional Proteomics Defines the Molecular Switch Underlying FGF Receptor Trafficking and Cellular Outputs. Mol Cell. 2013;51(6):707–722.

33. auf dem Keller U, et al. Systems-level analysis of proteolytic events in increased vascular permeability and complement activation in skin inflammation. Sci Signal. 2013;6(258):rs2.

34. Matsui T, et al. Identification of novel keratinocyte-secreted peptides dermokine-α/- β and a new stratified epithelium-secreted protein gene complex on human chromosome 19q13.1. Genomics. 2004;84(2):384–397.

35. Savage CR, Inagami T, Cohen S. The primary structure of epidermal growth factor. J Biol Chem. 1972;247(23):7612–21.

36. Bekker-Jensen DB, et al. Rapid and site-specific deep phosphoproteome profiling by data-independent acquisition without the need for spectral libraries. Nat Commun. 2020;11(1):1–12.

37. Xuan Y, et al. Standardization and harmonization of distributed multi-center proteotype analysis supporting precision medicine studies. Nat Commun. 2020;11(1):5248.

38. Watson J, et al. Spatially resolved phosphoproteomics reveals fibroblast growth factor receptor recycling-driven regulation of autophagy and survival. Nat Commun. 2022;13(1):6589.

670 39. Kim HJ, et al. PhosR enables processing and functional analysis of phosphoproteomic data. Cell Rep.
671 2021;34(8).

672 40. Etienne-Manneville S, Hall A. Rho GTPases in cell biology. Nature. 2002;420(6916):629–635.

673 41. Hall A. Rho GTPases and the Actin Cytoskeleton. Science (1979). 1998;279(5350):509–514.

674 42. Reynolds AB, Roczniak-Ferguson A. Emerging roles for p120-catenin in cell adhesion and cancer.
675 Oncogene. 2004;23(48):7947–7956.

676 43. Kourtidis A, et al. Distinct E-cadherin-based complexes regulate cell behaviour through miRNA processing
677 or Src and p120 catenin activity. Nat Cell Biol. 2015;17(9):1145–1157.

678 44. Kourtidis A, Ngok SP, Anastasiadis PZ. p120 catenin: an essential regulator of cadherin stability, adhesion-
679 induced signaling, and cancer progression. Prog Mol Biol Transl Sci. 2013;116:409.

680 45. Kauko O, et al. Label-free quantitative phosphoproteomics with novel pairwise abundance normalization
681 reveals synergistic RAS and CIP2A signaling. Scientific Reports 2015 5:1. 2015;5(1):1–17.

682 46. Dejana E, Orsenigo F, Lampugnani MG. The role of adherens junctions and VE-cadherin in the control of
683 vascular permeability. J Cell Sci. 2008;121(13):2115–2122.

684 47. Schmidt MF, et al. Pitfalls in the Application of Dispase-Based Keratinocyte Dissociation Assay for In Vitro
685 Analysis of Pemphigus Vulgaris. Vaccines (Basel). 2022;10(2).

686 48. Maiden SL, Petrova YI, Gumbiner BM. Microtubules Inhibit E-Cadherin Adhesive Activity by Maintaining
687 Phosphorylated p120-Catenin in a Colon Carcinoma Cell Model. PLoS One. 2016;11(2):e0148574.

688 49. Wu Q, et al. Monoubiquitination of p120-catenin is essential for TGFβ-induced epithelial-mesenchymal
689 transition and tumor metastasis. Sci Adv. 2020;6(4).

690 50. Chuang H-H, et al. Ser1333 phosphorylation indicates ROCKI activation. J Biomed Sci. 2013;20(1):83.

691 51. Hasegawa M, et al. Altered expression of dermokine in skin disorders. J Eur Acad Dermatol Venereol.
692 2013;27(7):867–875.

693 52. Shen X, et al. Nonlinear dynamics of multi-omics profiles during human aging. Nat Aging. 2024.

694 53. Mehta D, et al. The incongruity of validating quantitative proteomics using western blots. Nat Plants.
695 2022;8(12):1320–1321.

696 54. Kanitakis J, et al. Filaggrin expression in normal and pathological skin. A marker of keratinocyte
697 differentiation. Virchows Arch A Pathol Anat Histopathol. 1988;412(4):375–82.

698 55. Humphries EM, et al. Quantitative Comparison of Deparaffinization, Rehydration, and Extraction Methods
699 for FFPE Tissue Proteomics and Phosphoproteomics. Anal Chem. 2024;96(33):13358–13370.

56. Petrosius V, et al. Exploration of cell state heterogeneity using single-cell proteomics through sensitivity-tailored data-independent acquisition. Nat Commun. 2023;14(1):5910.

57. Lauridsen J, et al. InstaNovo-P: A de novo peptide sequencing model for phosphoproteomics [preprint]. 2025. https://doi.org/10.1101/2025.05.14.654049.

58. Jin X, et al. Functions of p120-catenin in physiology and diseases. Front Mol Biosci. 2024;11.

59. DeWane G, Salvi AM, DeMali KA. Fueling the cytoskeleton - links between cell metabolism and actin remodeling. J Cell Sci. 2021;134(3).

60. Kourtidis A, et al. Pro-Tumorigenic Phosphorylation of p120 Catenin in Renal and Breast Cancer. PLoS One. 2015;10(6):e0129964.

61. Mariner DJ, et al. Identification of Src Phosphorylation Sites in the Catenin p120. Journal of Biological Chemistry. 2001;276(30):28006–28013.

62. Uhlén M, et al. Tissue-based map of the human proteome. Science (1979). 2015;347(6220).

63. Nunan R, et al. Ephrin-Bs Drive Junctional Downregulation and Actin Stress Fiber Disassembly to Enable Wound Re-epithelialization. Cell Rep. 2015;13(7):1380–1395.

64. Eming SA, Martin P, Tomic-Canic M. Wound repair and regeneration: Mechanisms, signaling, and translation. Sci Transl Med. 2014;6(265).

65. Francavilla C, et al. Multilayered proteomics reveals molecular switches dictating ligand-dependent EGFR trafficking. Nat Struct Mol Biol. 2016;23(6):608–618.

66. Ahmadi S, et al. Proteomics and histological assessment of an organotypic model of human skin following exposure to Naja nigricollis venom. Toxicon. 2022;220:106955.

Figure legends

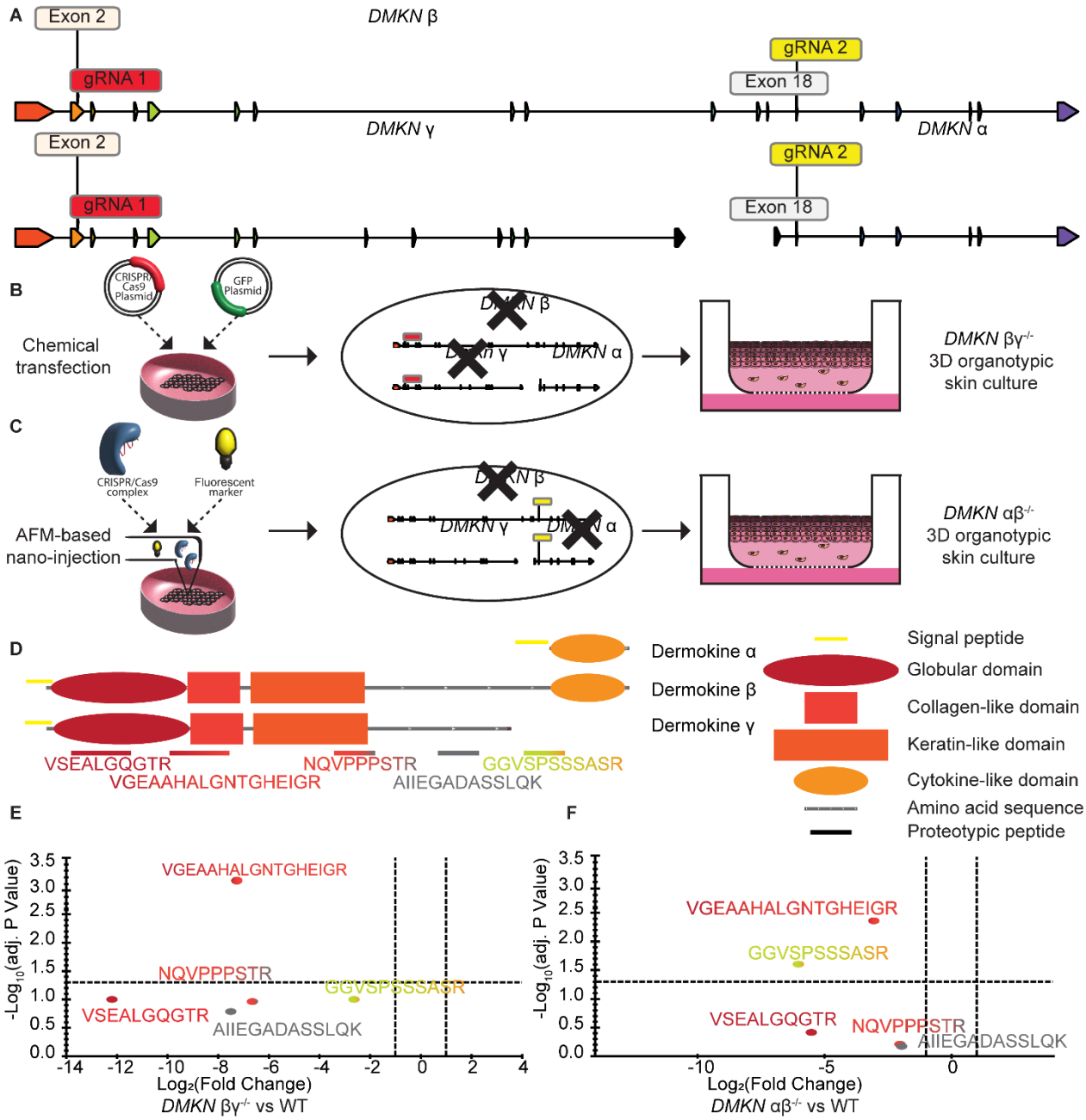

Figure 1: Targeted proteomics validates the knockout of dermokine in human keratinocytes. (A) Schematic of the genetic loci encoding the different dermokine isoforms and locations of guide RNAs (gRNA 1 and gRNA 2) targeting isoform-specific exons. **(B and C)** Methodologies used to delete dermokine in keratinocytes through either "chemical transfection" **(B)** or "FluidFM™ CRISPR approach". **(C)** After transfection and clonal expansion, WT, *DMKN* αβ$^{-/-}$ or *DMKN* βγ$^{-/-}$ keratinocytes were used for the generation of 3D organotypic skin cultures. **(D)** Schematic of the protein domains of the dermokine isoforms and of the five isoform-specific and proteotypic peptides used for targeted proteomics analysis. **(E and F)** Proteotypic dermokine peptide abundances are Log_2 transformed fold changes of summed transition areas from *DMKN* βγ$^{-/-}$ **(E)** or *DMKN* αβ$^{-/-}$ **(F)** relative to WT keratinocytes analyzed by targeted proteomics. N = 3 different 3D organotypic skin cultures. Statistical significance was calculated using two-sided Student's t-tests on

log_2-transformed intensities, with multiple-testing correction performed using the Benjamini–Hochberg false discovery rate.

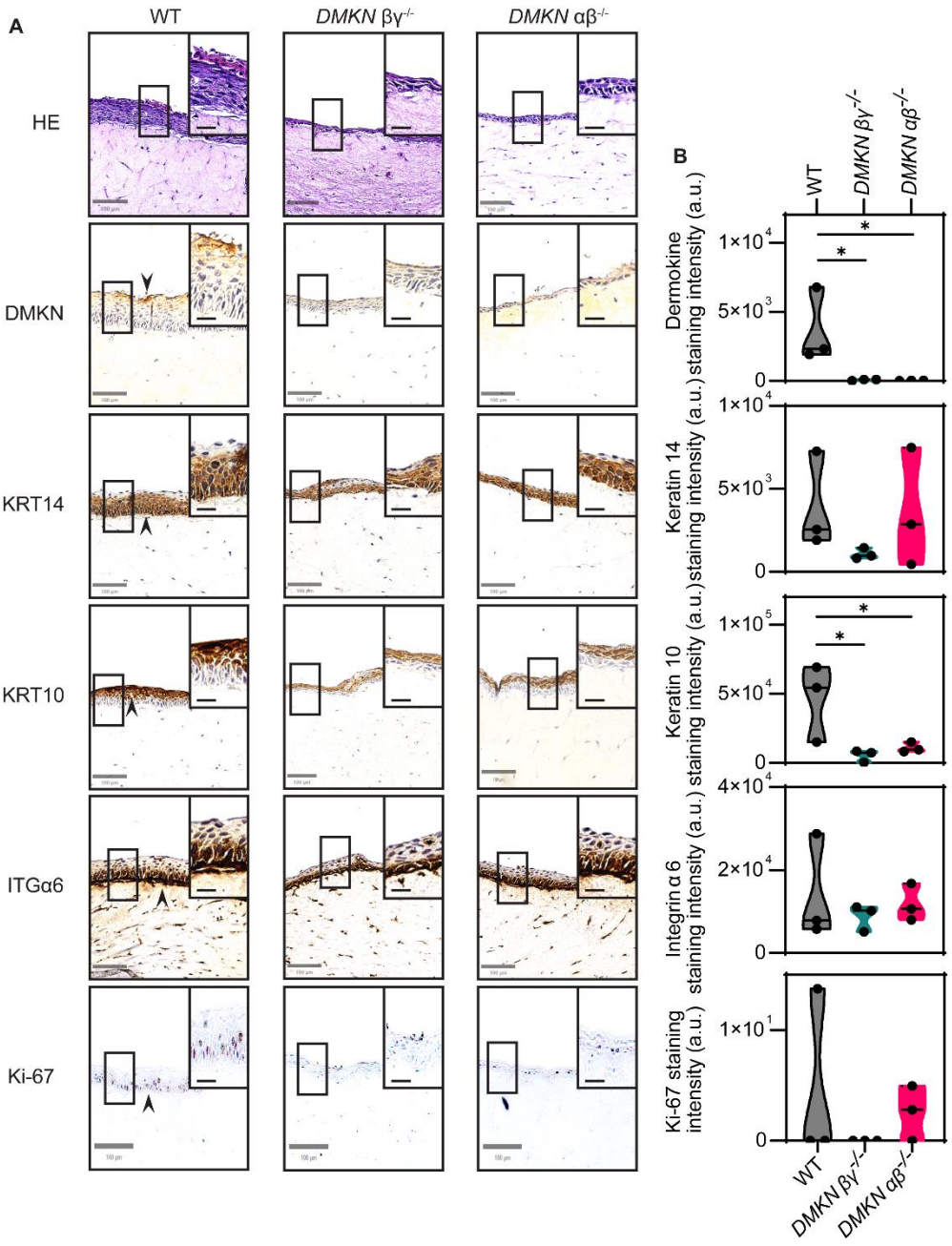

Figure 2: Staining of DMKN KO and WT 3D organotypic skin cultures shows changes in epidermal marker proteins. (A) H/E and IHC staining with the indicated antibodies of WT and *DMKN* $\alpha\beta^{-/-}$ or *DMKN* $\beta\gamma^{-/-}$ keratinocytes 3D organotypic skin cultures. N = 3, scale bar = 100 µm and scale bar (magnified images) = 25 µm. **(B)** Truncated violin plots showing the semi-quantitative immunohistochemical staining intensity with the indicated antibodies. N = 3 different 3D organotypic skin cultures. * = P < 0.05 (one-way ANOVA and a Fisher's Least Significant Difference test). a.u.: Arbitrary unit.

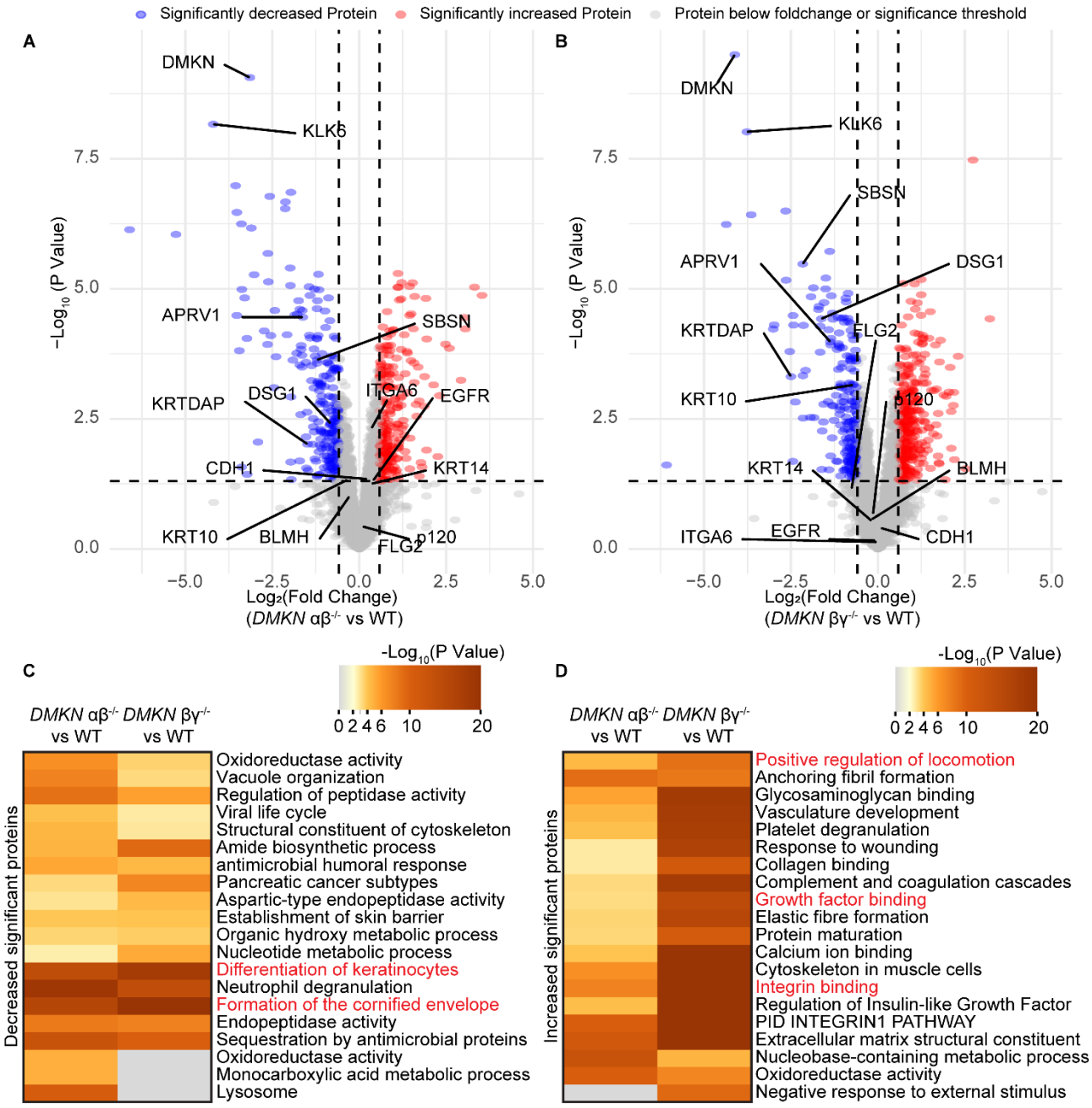

Figure 3: Proteomic analysis of dermokine-ablated 3D organotypic skin cultures shows phenotypic differences. (A and B) Volcano plots showing the differential protein abundance between *DMKN* αβ$^{-/-}$ **(A)** or *DMKN* βγ$^{-/-}$ **(B)** and WT keratinocytes in 3D organotypic skin cultures. Proteins characteristic for different epidermal strata are highlighted (1). Values are Log_2 transformed fold changes and -Log_{10} transformed p values (moderated contrast *t* test) of three different (3D) organotypic skin cultures. **(C and D)** Gene Ontology (GO) analysis of significantly decreased **(C)** or increased **(D)** proteins from *DMKN* αβ$^{-/-}$ **(A)** or *DMKN* βγ$^{-/-}$ **(B)** relative to the WT proteome.

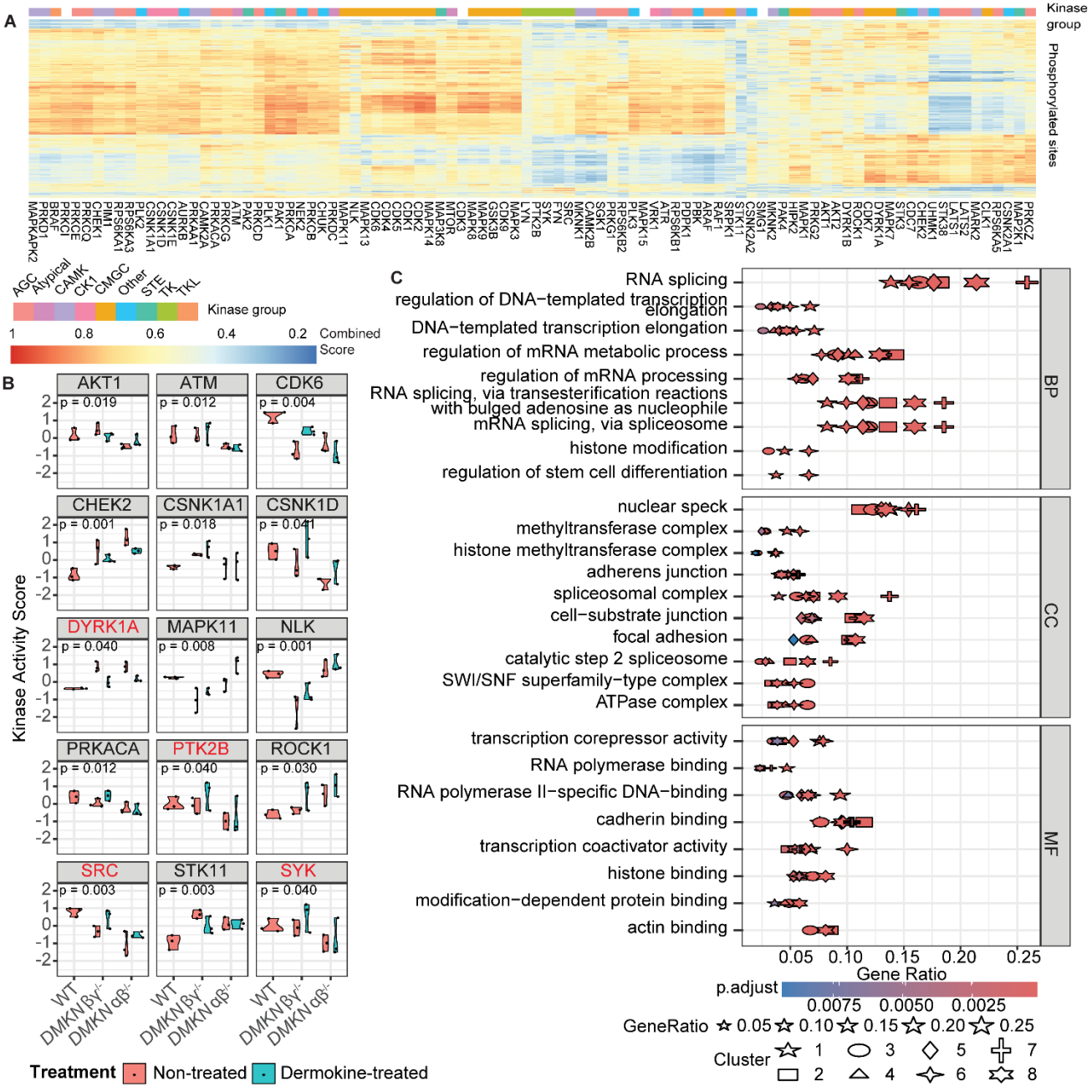

Figure 4: Absence of dermokine results in phosphorylation changes in adhesion proteins. (A) The Kinase-Substrate prediction approach(39) matched quantified phosphorylated sites in the WT and the two KO samples with the 94 identified putative kinases (Supplemental Table 5). The heatmap shows the combined score of the in vivo or in vitro kinases and sequence recognition motifs (39). Vertical axis shows substrates, and horizontal axis represents kinases. Family of kinases are color-coded on top of the graph. **(B)** The kinase activity score for *DMKN* $\alpha\beta^{-/-}$, *DMKN* $\beta\gamma^{-/-}$ and WT condition, treated with recombinant dermokine or vehicle, is shown for 15 significantly regulated kinases out of the 94 identified kinases. Values are kinase activity scores from N=3 technical replicates from the different genotypes and treatments. One-way ANOVA test determined changes among all genotypes. **(C)** Gene ontology analysis from proteins whose phosphorylated sites were annotated to kinases identified in clusters shown in Supplemental Figure 6.

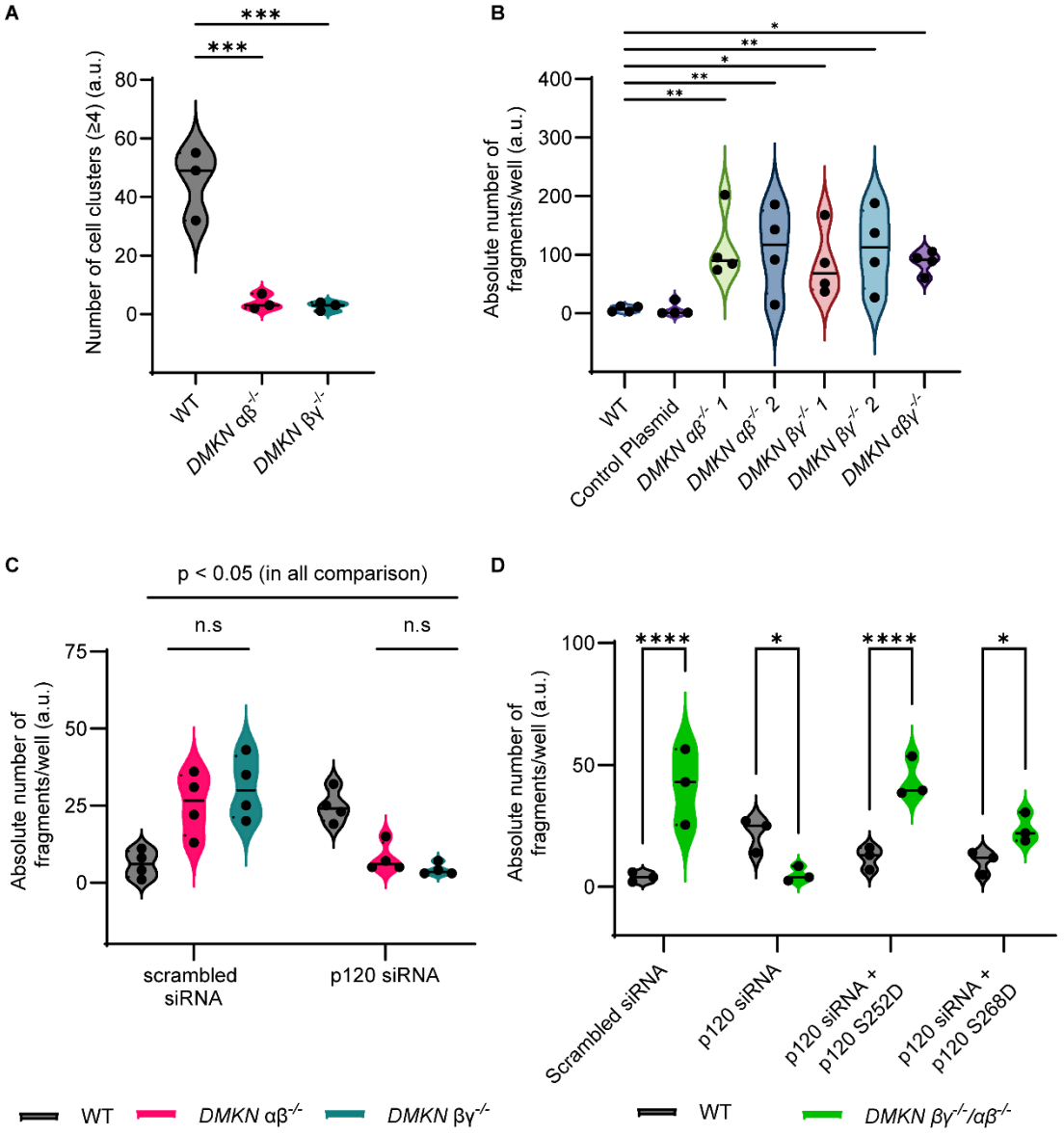

Figure 5: Cell-cell adhesion decreases in dermokine-depleted keratinocytes. **(A)** Quantification of 4 or more cell clusters from the cell-cell adhesion assay using *DMKN* αβ$^{-/-}$, *DMKN* βγ$^{-/-}$ and WT keratinocytes. Cell cluster (≥4) were counted, and each replicate was visualized as dot in the violin plot. N = 3 biological replicates. *** = P < 0.001 (one-way ANOVA and a Fisher's Least Significant Difference test). **(B)** Quantification of dispase dissociation assay data using independent clones of human *DMKN* αβ$^{-/-}$, *DMKN* βγ$^{-/-}$, *DMKN* αβγ$^{-/-}$, and WT keratinocytes transfected for 72 h with p120 or scrambled siRNA. Values are normalized to total fragment size. N = 4 biological replicates. * = P < 0.05, ** = P < 0,01 (one-way ANOVA and a Fisher's Least Significant Difference test). **(C)** Quantification of dispase dissociation assay data using *DMKN* αβ$^{-/-}$, *DMKN* βγ$^{-/-}$ and WT keratinocytes transfected for 72 h with p120 (1, 2 and 3), or scrambled siRNA. N = 4 biological replicates. All conditions are significant (P < 0.05) unless indicated otherwise (N.S.: P > 0.05) (two-way ANOVA and a Fisher's Least Significant Difference test). **(D)** Quantification of dispase dissociation assay data of *DMKN* αβ$^{-/-}$, *DMKN* βγ$^{-/-}$ and WT keratinocytes transfected for 48 h with p120 or scrambled siRNA followed by transfection with expression vectors encoding p120 mutants with an siRNA-resistant mutation and either S252D or S268D mutations. N = 3 biological replicates. * = P < 0.05, **** = P < 0.0001 (two-way ANOVA and a Fisher's Least Significant Difference test).

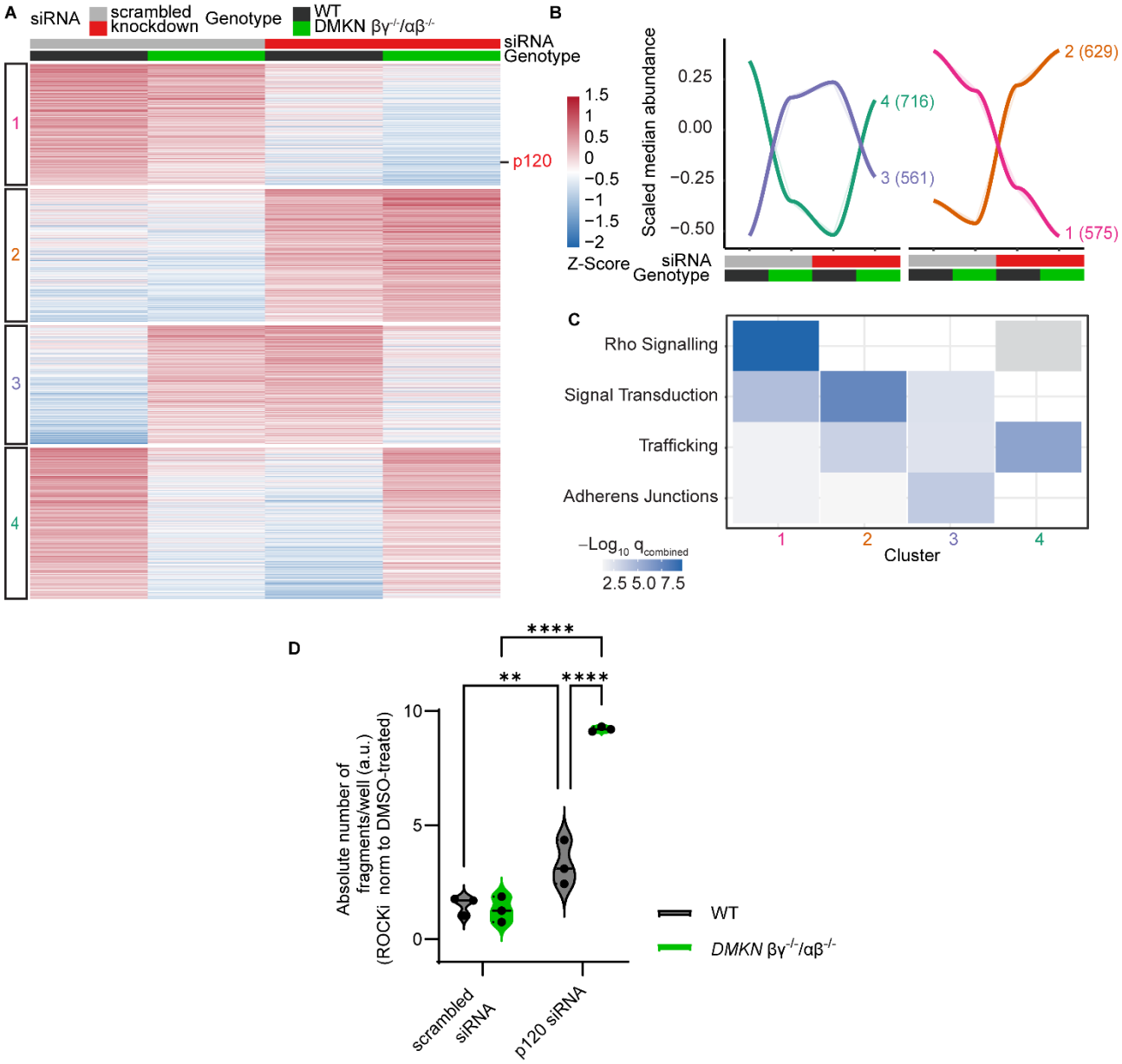

Figure 6: p120 perturbation and ROCK1 inhibition in keratinocytes regulate cell-cell adhesion. **(A)** Heatmap of the Z-scored differentially expressed proteins in the indicated genetic background show 4 distinct clusters. Genotypes and conditions are color-coded on top of the graph. **(B)** Lineplot of scaled abundances of all proteins within cluster from (A). Numbers indicate cluster number and total proteins for each cluster (in parentheses). **(C)** Pathway enrichment analysis of proteins in cluster 1, 2, 3 and 4. The color scale ($-Log_{10}(q_{combined})$) represents the aggregated and multiple-testing corrected significance of the module in each cluster. Shown are overhead terms and all terms can be found in Supplementary table 8. **(D)** Quantification of dispase dissociation assay using *DMKN* $\alpha\beta^{-/-}$, *DMKN* $\beta\gamma^{-/-}$ and WT keratinocytes transfected for 48 h with p120 or scrambled siRNA and treated with ROCK inhibitor for 24 hours. Data are normalized to DMSO treated values. N = 3 biological replicates. ** = P < 0.01, and **** = P < 0.0001 (two-way ANOVA and a Fisher's Least Significant Difference test).

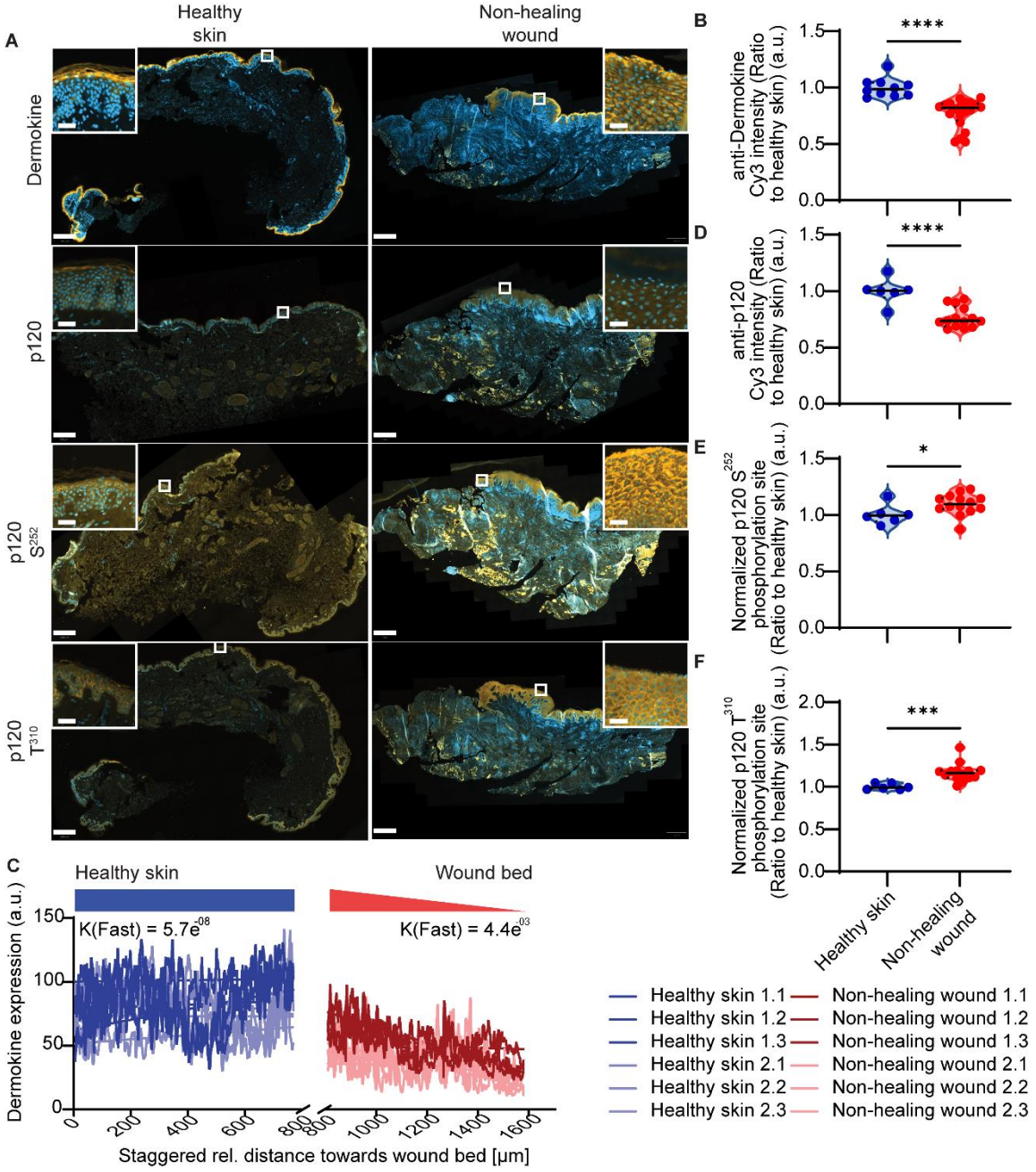

Figure 7: Dermokine expression decreases and p120 phosphorylation increases in keratinocytes non-healing wounds. (A) Representative images of immunofluorescent staining of biopsies from healthy skin around the breast tissue from healthy individuals and non-healing wounds of venous leg ulcers (Supplemental Table 6). **(B, D, E and F)** Quantification of immunofluorescent staining with the indicated antibodies from **(A)**. Anti-dermokine antibody values are the median Cy3 intensity values of N = 30 samples of four patients (non-healing wounds) and of six healthy individuals (healthy skin). Anti-p120 and anti-phosphorylated p120 antibodies values are median Cy3 intensity values of N = 20 samples of three patients (non-healing wound) and three patients (healthy skin). Scale bar for the healthy skin is 400 µm and for non-healing wounds 1 mm. The scale bar for the magnified images is 50 µm. * = P < 0.05, *** = P < 0.001, **** = P < 0.0001 (one-tailed, unpaired *t* test). **(C)** Quantification of dermokine intensity across 770,25 µm from the wound-edge towards healthy keratinocytes. The quantified area was measured in three horizontal rectangles across the epidermal profile (Supplemental Figure 9D). Values are Cy3 anti-dermokine intensities along 3 equally shaped rectangles placed within the same biological sample at two different anatomical sites

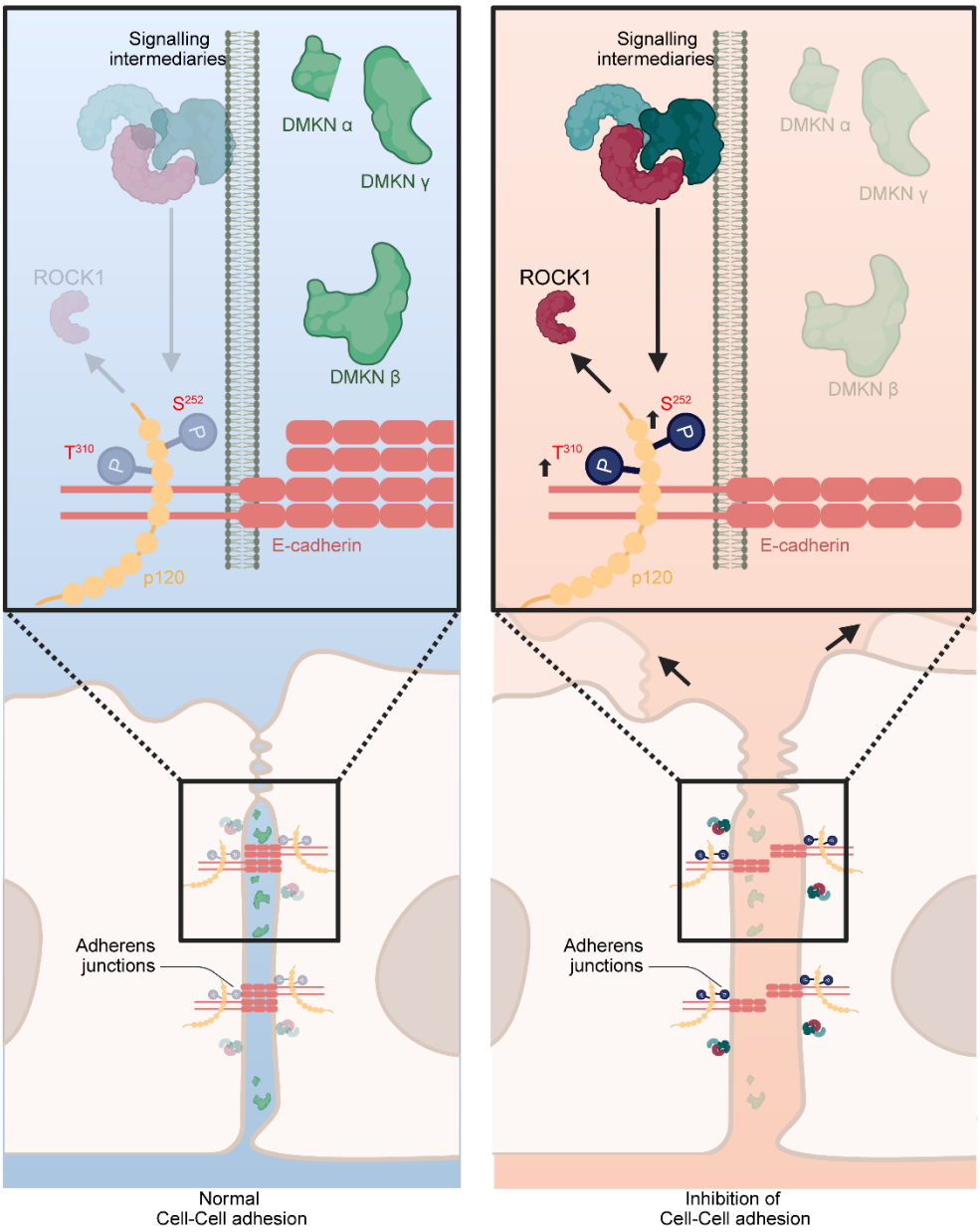

807

808 **Figure 8: Model of dermokine function in human keratinocytes.** Schematic of the putative relationship
809 between dermokine, cell-cell adhesion, and p120 phosphorylation created in Biorender.